5-1-2015

Visible and Infrared Spectroelectrochemistry of Zinc and Manganese Porphinones: Metal vs. Porphyrin Reduction

Florentina Tutunea
Marquette University

Abderrahman Atifi
Marquette University

Michael D. Ryan
Marquette University, michael.ryan@marquette.edu

Accepted version. *Journal of Electroanalytical Chemistry*, Vol. 744 (May 2015): 17-24. DOI.

Visible and Infrared Spectroelectrochemistry of Zinc And Manganese Porphinones: Metal Vs. Porphyrin Reduction

Florentina Tutunea
Chemistry Department, Marquette University
Milwaukee, WI
Abderrahman Atifi
Chemistry Department, Marquette University
Milwaukee, WI
Michael D. Ryan
Chemistry Department, Marquette University
Milwaukee, WI

Abstract: The visible and infrared spectroelectrochemistry of zinc and manganese porphinones and porphinediones was carried out in THF solutions. The aim of this work was to use FTIR spectroelectrochemistry and DFT calculation to determine whether the reduction was centered predominantly on the metal or the macrocycle. For zinc(II), the first one-electron reduction must occur on the macrocyclic ring because the metal's d-orbitals are filled (d^{10}). The carbonyl bands on the macrocyclic ring were used to probe the electronic structure because they can be readily observed in the infrared spectra. The results of this study are complementary to previous spectroelectrochemical studies that have been reported for the iron and cobalt complexes of the same macrocycles. As expected for the formation of a π-

Journal of Electroanalytical Chemistry, Vol. 744 (May 1, 2015): pg. 17-24. DOI.

radical anion species, significant downshifts in the carbonyl bands were observed. DFT calculations showed that the behavior of the porphinedione complexes were most sensitive to the electronic structure of the $M(OEPdione)^-$ species. If a M^I species is formed, the two carbonyl groups will be downshifted by similar energies. For M^{II}-radical anions, one carbonyl will be downshifted significantly, and the second one will be downshifted by a small amount. On the basis of this criterion, it was determined that cobalt(I) and iron(I) complexes were formed, while zinc and manganese formed π-radical anion species. The visible spectroelectrochemistry was also consistent with these electronic structures.

Graphical abstract: The visible and infrared spectroelectrochemistry of zinc and manganese porphinones and porphinediones was carried out in THF solutions. The carbonyl bands on the macrocyclic ring were used to probe the electronic structure. DFT calculations showed that the shifts in the carbonyl bands of the porphinedione (OEPdione) complexes were sensitive to the electronic structure of the $M(OEPdione)^-$ species. On this basis, the oxidation state of the metal in these complexes could be assigned.

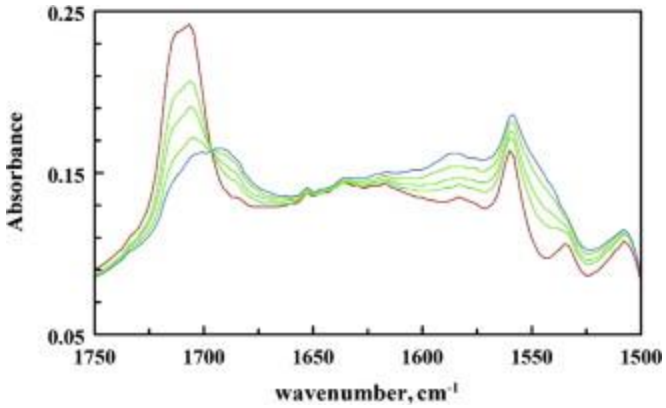

Keywords: DFT calculations; Porphinone; Cyclic voltammetry; Spectroelectrochemistry; Visible; Infrared

1. Introduction

The active site of several dissimilatory nitrite reductases contains heme d_1 as the prosthetic group. Heme d_1 is an iron porphinedione, one of the many unusual porphyrin prosthetic groups involved in the nitrogen cycle. The structure of heme d_1 was identified by Chang [1]. Work has been carried out in our laboratory

investigating the voltammetry, spectroelectrochemistry and reactivity of iron porphinones and porphinediones [2] and [3].

While visible spectroelectrochemistry can provide valuable information on the electronic structure of the low valent metal complexes, infrared spectroscopy can provide more definitive information. Previous work on cobalt porphyrin complexes has shown that the reduction of $Co^{II}(P)$ (where P = porphyrin) will lead to a $Co^{I}(P)^{-}$ complex [4]. On the other hand, $Zn^{II}(P)$ complexes are known to reduce to the porphyrin π-radical anion because zinc is a d^{10} complex. Zinc porphyrins (octaethylporphyrin, OEP, and tetraphenylporphyrin, TPP) have been extensively studied by voltammetry [5] and spectroelectrochemistry [5], [6] and [7]. The resonance Raman spectroscopy of $Zn(P)^{-}$ has also been reported [7] and [8]. Unlike the zinc complex, there have been fewer studies carried out on the reduction of $Mn^{II}(P)$ complex. Fuhrhop et al. [9] characterized $Mn(P)^{-}$ as a manganese(II) radical anion, as did Kelly and Kadish [10] and Boucher and Garber [11]. Additional information confirming the radical anion structure was provided by Guldi et al. [12], who observed a broad absorption band around 770 nm, which is characteristic of porphyrin π-radical anions. On the other hand, DFT calculations by Liao and Huang [13] predicted a Mn(I) structure for manganese porphine.

The aim of this work will be to use infrared spectroelectrochemistry along with DFT calculations in order to correlate the changes in the infrared spectra with the electronic structure of the formal M(I)-porphyrin or M(II) π-radical anion complex. Reduction of zinc porphinones should reveal features in the infrared and visible typical of π-anion radicals, as zinc is a d^{10} complex. The previous work on cobalt porphinones has allowed us to obtain spectra characteristic of a metal reduction [14]. Using the insight gained from these two metals, the spectroelectrochemistry of manganese and iron [15] can be better understood. There still remains considerable controversy as to the electronic structure of the $Fe^{I}(P)^{-}$ complex. This investigation should help clarify this issue. The carbonyl group, which is present on the macrocycle, can be easily observed with infrared spectroscopy, and is sensitive to the degree of delocalization of the metal electron density onto the macrocycle. The magnitude of

the shift and the behavior of the two carbonyl groups in the porphinediones upon reduction should provide this insight.

2. Experimental

2.1. Chemicals

Octaethylporphyrin (H_2OEP) was purchased from Sigma–Aldrich Chemical Co. Tetrabutylammonium perchlorate (TBAP) was purchased from Alfa Aesar and dried at 90 °C in a vacuum oven overnight. Bis(triphenylphosphine)iminium chloride (PNPCl) was obtained from Sigma–Aldrich Chemical Co. Anhydrous tetrahydrofuran (THF) was refluxed in the presence of sodium and benzophenone under nitrogen until the solution was blue. The solution was deoxygenated at least three times by freeze–pump–thaw cycles before being used in the glove-box. All other solvents were spectrophotometric grade and used without further purification. Octaethylporphinone (H_2OEPone) and octaethylporphinedione (H_2OEPdione) were synthesized by literature methods [16], [17] and [18]. The ZnOEPone was prepared by a two-step reaction via OsO4 oxidation of ZnOEP and acid catalyzed pinacolic rearrangement using the literature method published by Chang et al. [16], [18] and [19]. This reaction gave a mixture of unreacted H_2OEP, ZnOEPone and 2,6-OEPdione. After removing the solvent, the mixture of zinc complexes was purified using an alumina column and elution was initiated with chloroform. A small violet band containing free base 2,6 porphinedione, H_2(2,6-OEPdione), which did not react with zinc acetate, eluted first. The second band containing ZnOEP (pink) from unoxidized starting material was eluted with chloroform containing 0.5% methanol. The third band (blue) was eluted with chloroform containing 5% methanol, which contained ZnOEPone. The manganese porphinone complexes were synthesized using manganese acetate tetrahydrate, sodium acetate, and sodium chloride in acetic acid. The mixture was heated at reflux for 24 h. The resulting solution was cooled at room temperature, reduced to a volume of less than 5 mL, and washed 3 times with 100 mL of water, 5%$NaHCO_3$ solution (2 × 100 mL), then once more 3 times with 100 mL of water. The crude manganese complex was purified using an alumina column. Elution started with chloroform to remove the unreacted material and continued with chloroform containing 1% methanol.

To obtain zinc and manganese porphinediones, the H_2(2,4-OEPdione) compound was allowed to react with the corresponding metal acetates in $CHCl_3$/MeOH (20/10 mL) at reflux for 1 h, in case of zinc, or 24 h for manganese. The completion of the reaction was monitored using thin layer chromatographic techniques. Silica gel TLC plates were immersed in a solvent mixture of hexane:dichloromethane (1:1 ratio). The resulting solution was cooled at room temperature and washed 3 times with 300 mL of water. After removing the solvent, the crude metal complex was purified on silica gel column. Elution was initiated with chloroform.

2.2. Equipment

The UV–visible spectra were recorded on a Hewlett-Packard 8452A diode array spectrophotometer with an OLIS data acquisition system. An optically transparent thin layer electrode (OTTLE) cell was used for visible spectroelectrochemistry. The cell assembly was based on the design of Lin and Kadish [20]. A silver wire was used as a reference electrode. The electrode potentials that corresponded to each spectra were obtained using an E-corder (eDAQ Pty Ltd., Australia), which was controlled by the software program, Chart (eDAQ). Each time that the diode array slit opened, the E-corder was triggered to acquire the potential from the potentiostat. The potentials recorded in this work were the average potentials during the spectral acquisition time. The infrared spectra were obtained with a Thermo Nicolet-FTIR spectrophotometer (Model 670 Nexus) with a MCT detector. Infrared spectra of solid materials were collect as KBr pellets. The FTIR OTTLE cell has been described previously [15].

2.3. Procedures

All samples for spectroelectrochemical analysis were prepared and the cells filled in the glove box under argon. The supporting electrolyte was 0.10 M TBAP. FTIR spectra were obtained using 32 scans, and 2 cm^{-1} resolution unless noted differently. The UV–visible spectra were obtained from cyclic scans of the potential, while FTIR spectra were obtained at constant potential. All potentials are reported vs. SCE (V vs. SCE = V vs. Ag/$AgClO_4$ + 0.36 V). In some cases, small amounts of residual starting material could be observed in the final

spectrum due to the fact that the working electrode did not cover the entire beam. In these cases, the residual amounts were digitally subtracted in order to obtain the final spectrum of the oxidized/reduced species. For all the spectroelectrochemical experiments (visible and infrared), the potential was returned to the initial potential after the experiment was completed in order to verify that the starting spectrum could be recovered. This indicated that an irreversible chemical reaction had not occurred. This condition was fulfilled for all reported spectra.

2.4. Computation

Electronic structure and vibrational spectral calculations were carried out using the m06 or the bp86 DFT functionals and the TZVP basis set for all elements except for the transitional metal using the Gaussian 09 suite of programs [21]. The TZVP basis set was also used for zinc. The Wachters' basis set was used for manganese, iron and cobalt [22]. All calculations converged using the tight optimization criteria. The high-spin $Mn(P)^{-}$ complexes were all solved using the anti-ferromagnetic coupling procedure available at the Gaussian website. Two fragments were used in the calculation: Mn^{II} (high spin, sextet) and the macrocycle (−3 charge, doublet), antiferromagnetically coupled. A plot of observed and calculated ν_{CO} wavenumbers of M(II) and M(III) porphinones (where M is the metal) for the m06 functional is shown in Fig. S1 of the Supporting information. All the calculated wavenumbers were about 6% higher than the experimental values. As a result, a scale factor of 0.94 was used for the ν_{CO} values. The porphyrin vibrations, as calculated by the m06 functional, were closer to the experimental values and a scale factor of 0.97 was more appropriate. Complementary calculations were performed using the bp86 functional. The carbonyl vibrational energy was always underestimated by this functional, but not in a fashion that could be corrected by a scale factor. The observed ν_{CO} values were 13 ± 6 cm^{-1} lower than the experimental values. No scale factor was used for this functional, but comparisons between the experimental data and the bp86 predicted values should be interpreted in light of this tendency. The redox potentials for the metalloporphinones were calculated using the method of Holland et al. [23].

Journal of Electroanalytical Chemistry, Vol. 744 (May 1, 2015): pg. 17-24. DOI.

3. Results and discussion

3.1. Voltammetry of zinc porphinones

Zinc(II) porphyrins and porphinones were reduced by one electron to the π-radical anion at about −1.6 V vs. SCE in THF. The results are summarized in Table 1. Further reductions occur at more negative potentials, but this work will focus only on the first reduction wave. The voltammetric data for zinc porphinones is summarized in Table 1. As was observed for cobalt and iron porphinones, the $E_{1/2}$ for porphinone complexes were positive of the $E_{1/2}$ of the OEP complexes. The $E_{1/2}$ for Zn(OEPone) was about 194 mV positive of the $E_{1/2}$ for Zn(OEP) (literature values are somewhat lower due to different reference electrodes/solvents/electrolytes, but the differences are similar: 230 mV). This compares with a value of 317 mV from DFT calculations for THF using the PCM method. By contrast, the second carbonyl group shifted the $E_{1/2}$ in the other direction, making the reduction of Zn(OEPdione) 75 mV more negative than Zn(OEPone). This is close to the value predicted by DFT (62 mV). The trend in potentials for Zn(OEPone)/Zn(OEPdione) is different from what was observed for iron (Fe(OEPdione), where the dione $E_{1/2}$ was 80 mV positive of the $E_{1/2}$ for Fe(OEPone) [3]). Smaller differences were observed for cobalt octaethylporphinone/octaethylporphinedione (+10 mV) [14]).

Table 1. Cyclic voltammetric data for metalloporphinones.[a]

Compound	$E_{1/2,metal}$	$E_{1/2,ring}$	References
Zn(OEP)	–	−1.761 V	This work
	–	−1.61 V[b]	[9]
Zn(OEPone)	–	−1.567 V	This work
	–	−1.38 V[c]	[24]
Zn(OEPdione)	–	−1.642 V	This work
Mn(OEP)Cl	−0.347 V	−1.736 V	This work
Mn(OEPone)Cl	−0.194 V	−1.369 V	This work
Mn(OEPdione)Cl	−0.116 V	−1.656 V	This work

[a] V vs. SCE; data from this work were obtained using 0.1 M $Ag/AgNO_3$ in acetonitrile as the reference electrode. All data were corrected by subtracting 0.360 V. Solvent: THF; supporting electrolyte: 0.10 M TBAP; working electrode: platinum.
[b] In 0.10 M TBAP/DMSO.
[c] In 0.10 M TBAP/acetonitrile.

Journal of Electroanalytical Chemistry, Vol. 744 (May 1, 2015): pg. 17-24. DOI.

3.2. Visible spectroelectrochemistry of zinc porphinones

The spectroelectrochemistry Zn^{II}(OEP) has been previously reported [24], and the spectra are summarized in Table 2. The reduction of Zn^{II}OEPone (Fig. S2) displayed a significant decrease in the Soret band which was shifted toward longer wavelength (418–450 nm) while the Q band at 620 nm was bleached. In addition, a weak broad band appeared around 650 nm. Isosbestic points were observed at 360 and 430 nm, indicating only two spectral species were present. These changes are consistent with the formation of a π-radical anion. The initial ZnOEPone spectrum was regenerated by re-oxidation, indicating that the one electron reduction product was stable on the timescale of the experiment.

Table 2. Visible spectra of metalloporphyrins and metalloporphinones.

Compound	Solvent	Soret band (nm)	Other bands (nm)	References
Zn(OEP)	THF	408	538, 572	[7]
$Zn(OEP)^-$	THF	452		[7]
Zn(OEPone)	Benzene	402, 418	572, 621	[24]
	THF	400, 418	572, 620	This work
$Zn(OEPone)^-$	THF	450	650	This work
Zn(OEPdione)	THF	390, 414, 440	624	This work
$Zn(OEPdione)^-$	THF	400, 402, 482	626, 688	This work
Mn(OEP)Cl	THF	364, 464		This work
Mn(OEP)	THF	418	544	This work
$Mn(OEP)^-$	THF	454		This work
Mn(OEPone)Cl	THF	364, 478	642	This work
Mn(OEPone)	THF	440	576, 624	This work
$Mn(OEPone)^-$	THF	444	680	This work
Mn(OEPdione)Cl	THF	366	504, 646	This work
Mn(OEPdione)	THF	402, 436, 464	590, 628	This work
$Mn(OEPdione)^-$	THF	406, 466	500 (sh), 680	This work

The visible spectrum of Zn^{II}OEPdione is shown in Fig. 1. A strong Soret band at 440 nm was observed along with smaller bands at 390 and 414 nm, and a Q band at 624 nm (band around 590 nm is due to light scattering by the grid electrode). Controlled potential reduction of the complex at −1.69 V in a thin layer spectroelectrochemical cell led to a significant decrease in the Soret

band while the Q band was almost bleached (Fig. 1). The significant decrease in the Soret band and the appearance of a broad long wavelength band at 688 nm to replace the Q band are indications of a π-radical anion formation. The isosbestic points at 436 and 450 nm indicate that intermediates were not formed. Unlike Zn^{II}OEPone, the band at 624 nm did not completely disappear but shifted to 626 nm. The re-oxidation of the singly reduced species led to complete recovery of the initial visible spectrum.

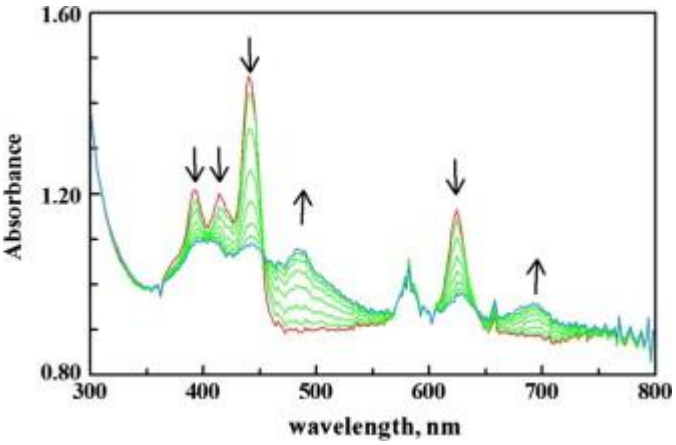

Fig. 1. Visible spectroelectrochemistry for the reduction of 0.80 mM Zn(OEPdione) in THF with 0.10 M TBAP. Red line is the initial scan; blue line is the final scan; green lines are the intermediate spectra. Scan rate = 8.2 mV/s; E_i = −0.30 V; E_f = −1.60 V vs. Ag wire. (For interpretation of the references to colour in this figure legend, the reader is referred to the web version of this article.)

A comparison of the zinc porphyrins from the literature with the zinc porphinones and porphinedione in this work revealed that the spectral changes in the electroreduction occur in the same visible region and correspond to features representative of π-radical anion formation. The addition of one electron into the system led to significant decreases in the Soret band and to the appearance of broad band in the visible regions which are characteristic of the formation of π-radical anions. Interestingly, unlike other radicals, a broad long wavelength absorption was not observed for the $Zn(OEP)^{-}$, but the band was observed for zinc porphinone radicals.

Journal of Electroanalytical Chemistry, Vol. 744 (May 1, 2015): pg. 17-24. DOI.

3.3. Infrared spectroelectrochemistry of zinc porphinones

The KBr mid-infrared spectrum of Zn(OEPone) contains a strong band at 1709 cm^{-1}, as well as a second band at 1686 cm^{-1}. This band was also observed by Stolzenberg et al. [24], and was considered to be a carbonyl band. When the compound was dissolved in THF, the 1709 cm^{-1} remained but the 1686 cm^{-1} band observed in the crystal disappeared. This lower energy band is probably due to packing forces in the solid. All the other porphinone complexes studied, as well as the freebase porphinone yielded only a single carbonyl band in the mid-IR region. In addition to the carbonyl band, two strong bands were observed at 1558 and 1536 cm^{-1}. These bands were also observed in THF solutions. Weaker bands were observed at 1581 and 1491 cm^{-1}. The KBr and solution mid-IR data are summarized in Table 3.

Table 3. Mid-infrared spectra of metalloporphinones.

Compound	Media	ν_{CO} (cm^{-1})	Other bands (cm^{-1})	References
Zn(OEPone)	KBr	1709, 1686		[24]
	KBr	1709, 1688	1581, 1558, 1536, 1491	This work
	THF	1709	1558, 1534	This work
$Zn(OEPone)^-$	THF	1662	1590, 1550, 1540	This work
Zn(OEPdione)	KBr	1718, 1668	1560, 1540, 1494, 1456, 1396, 1380, 1355, 1321, 1297, 1269, 1224, 1215, 1200	This work
	THF	1713, 1706	1560, 1534	This work
$Zn(OEPdione)^-$	THF	1690	1585, 1570, 1550	This work
Mn(OEPone)Cl	KBr	1718	1592s, 1577,1541, 1507, 1481, 1464, 1458, 1397, 1376, 1317, 1309, 1263, 1228, 1214	This work
	THF	1721	1578, 1570, 1542	This work
Mn(OEPone)	THF	1707	1542	This work
$Mn(OEPone)^-$	THF	1657	1582, 1542, 1527	This work
Mn(OEPdione)Cl	KBr	1719	1593, 1570, 1546, 1538, 1457, 1401, 1380, 1352, 1297, 1263, 1225, 1214, 1200	This work
	THF	1726, 1718	1595, 1570	This work

Compound	Media	ν_{CO} (cm^{-1})	Other bands (cm^{-1})	References
Mn(OEPdione)	THF	1710, 1704	1552, 1522	This work
$Mn(OEPdione)^-$	THF	1693	1600, 1568, 1552	This work

Thin layer FTIR spectroscopic data were collected during the electroreduction of ZnOEPone and the results are shown in Fig. 2 and Table 3. Upon reduction, the carbonyl band shifted from 1709 cm^{-1} to 1662 cm^{-1}, and three new bands were observed at 1590, 1550 and 1540 cm^{-1}. The bands at 1558 and 1534 cm^{-1} disappeared. Almost complete recovery of the original spectrum was obtained upon re-oxidation. The presence of isosbestic points during the reduction indicated that no intermediates were formed.

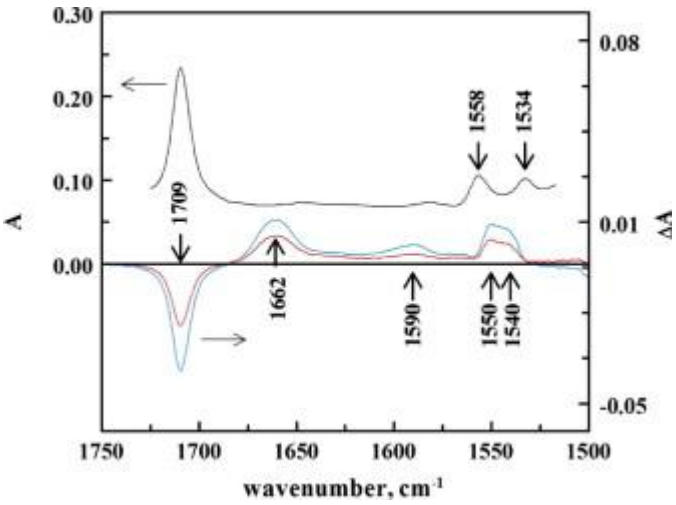

Fig. 2. Infrared spectroelectrochemistry for the reduction of 3.0 mM Zn(OEPone) in THF with 0.10 M TBAP. Black line: Spectrum of Zn(OEPone) (background subtracted); red line is the intermediate difference spectrum; blue line is the final difference spectrum; E = −1.60 V vs. Ag wire; 32 scans; 1 cm^{-1} resolution. (For interpretation of the references to colour in this figure legend, the reader is referred to the web version of this article.)

The reduction of ZnOEPdione was also examined by infrared spectroelectrochemistry. As was observed for Zn^{II}(OEPone) in KBr, an additional band was observed for Zn^{II}(OEPdione) at 1668 cm^{-1}. This band also disappeared in THF, but two carbonyl bands were still observed for the dione, at 1713 and 1706 cm^{-1}. In addition, other bands were observed at 1560 and 1534 cm^{-1} (Fig. 3). Upon reduction, the carbonyl band shifted to 1690 cm^{-1}. New bands were observed at 1585, 1570 and 1550 cm^{-1}, and the band at 1560 cm^{-1} decreased,

and shifted for 1558 cm^{-1}. The presence of isosbestic points during the reduction indicated that no significant decomposition of the product had occurred. Significantly, the reduction of the ZnOEPdione complex led to a much smaller downshift in the carbonyl band (23 cm^{-1}) as compared to the ZnOEPone complex (45 cm^{-1}). As with the ZnOEPone complex, reoxidation regenerated the starting material with isosbestic points.

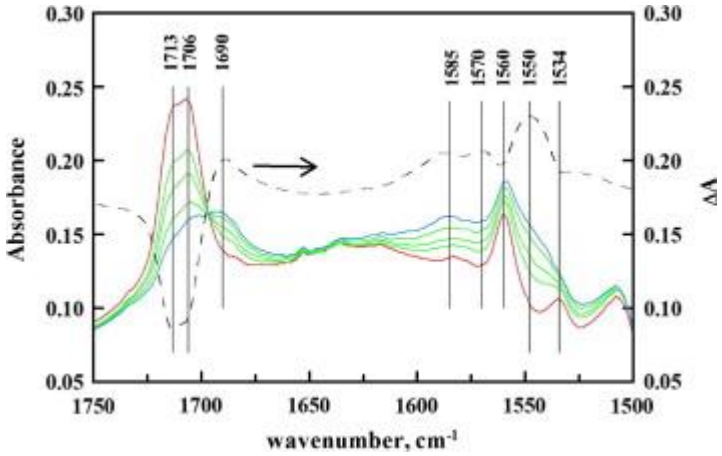

Fig. 3. Infrared spectroelectrochemistry for the reduction of 3.0 mM Zn(OEPdione) in THF with 0.10 M TBAP. red line: initial spectrum of Zn(OEPdione) (background subtracted); green lines: intermediate spectra; blue line is the final spectrum; dashed black line is the difference spectrum between the first and last spectra; E = −1.60 V vs. Ag wire. (For interpretation of the references to colour in this figure legend, the reader is referred to the web version of this article.)

3.4. DFT calculation of the infrared spectra

All of the DFT calculations were performed using the m06 and/or the bp86 functionals, as described in the Section 2. The results of the calculations for Zn(II) porphinones and their reduction products are shown in Table 4, along with values from the literature. The m06 functional with a scale factor of 0.94 correctly predicts the ν_{CO} for Zn(OEPone) and Zn(OEPdione). As is typical of previous work, the bp86 functional predicts values that are about 10 cm^{-1} low. The spectrum for $Zn(OEPone)^-$ between 1500 cm^{-1} (cutoff for THF) to 1800 cm^{-1} is shown in Fig. S3. The m06 functional does a better job of reproducing the observed spectrum than the bp86 functional in this case. The reduction of Zn(OEPone) to $Zn(OEPone)^-$ caused a 45 cm^{-1} downshift in the ν_{CO} vibration. This is reasonable close to the predicted values (58 cm^{-1} for m06 and 44 cm^{-1} for bp86). The spin density plot

for Zn(OEPone)$^-$ (m06) is shown in Fig. S4 of the Supporting information, which confirms a π-radical anion structure for the reduction product. The reduction of Zn(OEPdione) to Zn(OEPdione)$^-$ showed more nuanced shifts. DFT calculations showed that one carbonyl band has a small decrease in energy (DFT: 1718 to 1695 cm^{-1}, experimental: 1713 to 1690 cm^{-1}), which was seen in the spectrum. In addition, DFT calculations show that the second carbonyl downshifts more dramatically (DFT: 1708 to 1617 cm^{-1}, experimental: 1706 to 1585 cm^{-1}). As a result, unlike the M(III) and M(II) complexes of porphinediones, there was a significant split in the vibrational energy of the two carbonyl groups in the reduced product. This behavior is correctly predicted by the m06 functional (1695 and 1617 cm^{-1}), but not by the bp86 functional (1649 and 1622 cm^{-1}). The spin density diagram for Zn(OEPdione)$^-$ for the m06 functional is shown in Fig. 4A. The left carbonyl in the figure has very little spin density and is little affected by the reduction of the complex, while the right carbonyl has considerable spin density, which led to a downshift in its energy. An examination of the spin density plot for the bp86 functional on the other hand showed considerable spin density on both carbonyls.

Table 4. Experimental and calculated carbonyl vibrations of metalloporphinones.

	bp86 (cm^{-1})	**m06 (cm^{-1})[a]**	**Experimental (cm^{-1})**
Zn(OEPone)	1693	1708	1709
Zn(OEPone)$^-$	1649	1650	1662
Zn(OEPdione)	1703, 1698	1718, 1708	1713, 1706
Zn(OEPdione)$^-$	1649, 1622	1695, 1617	1690, 1585
Mn(OEPone)Cl	1697	1716	1721
Mn(OEPone)	1688	1709	1707
Mn(OEPone)$^-$	1648	1654	1657
Mn(OEPdione)Cl	1703, 1699	1732, 1717	1726, 1718
Mn(OEPdione)	1692, 1680	1717, 1707	1710, 1704
Mn(OEPdione)$^-$	hs: 1635, 1619	hs: 1593, 1684 ls: 1665, 1651	1693, 1600
Co(OEPone)Cl	1696	1719	1715
Co(OEPone)	1700	–	1709
Co(OEPone)$^-$	1654	1666	1674
Co(OEPdione)Cl	1706, 1703	1725, 1713	1721
Co(OEPdione)	–	–	1709

Journal of Electroanalytical Chemistry, Vol. 744 (May 1, 2015): pg. 17-24. DOI.

	bp86 (cm^{-1})	m06 (cm^{-1})[a]	Experimental (cm^{-1})
$Co(OEPdione)^-$	–	1647, 1638	1683, 1668
Fe(OEPone)Cl	1698	1717	1719
$Fe(OEPone)(THF)_2$	1686	–	1703
$Fe(OEPone)^-$	1643, 1608	1655	1671
Fe(OEPdione)Cl	1699, 1695	1721, 1715	1717
$Fe(OEPdione)(THF)_2$	1693, 1679	1712, 1706	1703
$Fe(OEPdione)^-$	1659, 1647	1695, 1652	1662, 1657

[a] Scale factor = 0.94.

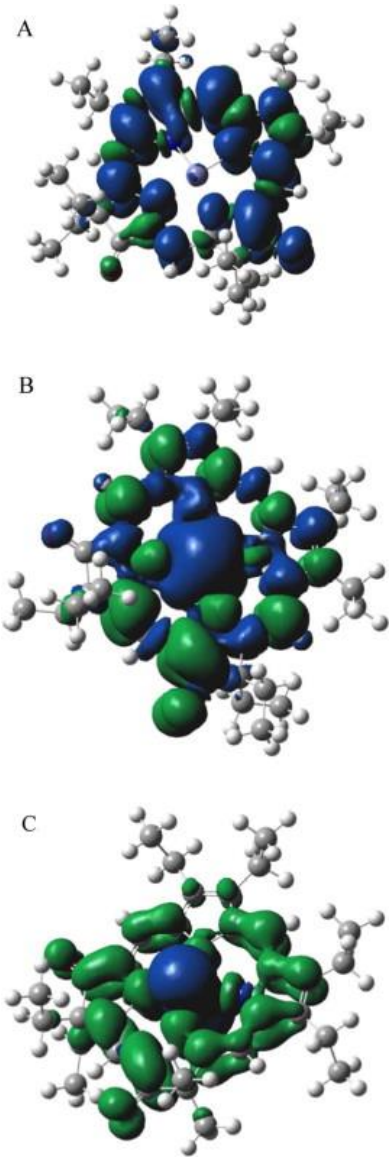

Fig. 4. Spin densities for $Zn(OEPdione)^-$ (A), $Mn(OEPdione)^-$ (B), and $Fe(OEPdione)^-$ (C), calculated using Gaussian 09 with DFT and m06 functional.

The two bands at 1558 and 1534 cm^{-1} were porphyrin core vibrations in Zn(OEPone). DFT calculations (m06) showed that the 1558 cm^{-1} vibration (1559 cm^{-1} in DFT calculations) were predominately $C_a–C_m–C_a$ antisymmetric stretches. The 1534 cm^{-1} vibration (1530 cm^{-1} in DFT calculations) was $C_a–C_m–C_a$ on the two meso-carbons bonded to the pyrrole with the carbonyl. Upon reduction, three bands were observed (1590, 1550 and 1540 cm^{-1}). Based on the modes for the 1534 cm^{-1} vibration, the 1540 cm^{-1} corresponded to the 1534 cm^{-1} vibration in the neutral zinc porphinone. The 1550 cm^{-1} band best corresponded to the 1558 cm^{-1} band, while the 1590 cm^{-1} band was a very weak band in the neutral zinc porphyrin complex (DFT: 1571 cm^{-1}). Upon reduction, the carbonyl vibration couples better with the core vibrations and its absorbance increases significantly. DFT calculations predict another band at 1567 cm^{-1} which may be the cause of the broadening of the observed band. The important point is that reduction led to a significant decrease in the ν_{CO} band, which can lead to an enhancement of the core vibrations as they can now couple with the $C = O$ vibration.

3.5. Voltammetry of manganese porphinones

The reduction of manganese porphinones occurs in two reversible one electron waves (Fig. 5). In order to obtain a reversible first reduction wave, chloride as PNPCl was added to the solution. Previous work has shown that chloride remains coordinated with the manganese upon reduction from manganese(III) to manganese(II) in the presence of excess chloride [25] and [26].

$$\mathrm{Mn^{III}(P)(Cl) + e^- \rightarrow Mn^{II}(P)(Cl)^-} \quad \mathrm{E_{1/2,1}}$$

$$\mathrm{Mn^{II}(P)(Cl)^- + e^- \rightarrow Mn(P)^- + Cl^-} \quad \mathrm{E_{1/2,2}}$$

Journal of Electroanalytical Chemistry, Vol. 744 (May 1, 2015): pg. 17-24. DOI.

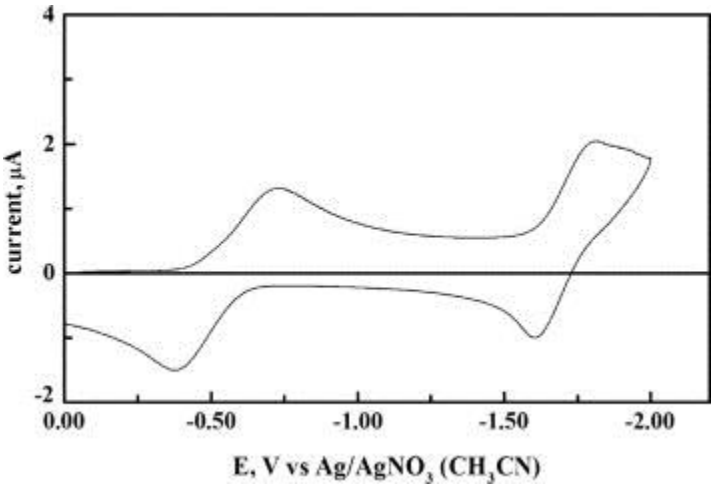

Fig. 5. Cyclic voltammetry of 0.50 mM Mn(OEPone)Cl in THF. Scan rate = 0.10 V/s, working electrode: Pt; reference electrode: $Ag/AgNO_3$ in acetonitrile. 5.0 mM PNPCl added.

Over the range from 5 to 20 mM chloride, the $E_{1/2,1}$ was independent of the chloride concentration (added as PNPCl) indicating that the chloride ion remained ligated to Mn under these conditions. In the absence of added chloride, Mn^{II}(OEPone) and Mn^{II}(OEPdione) were uncoordinated with chloride, based on the apparent quasi-reversibility of the wave (due to an EC mechanism). The $E_{1/2,2}$ for Mn^{II}(OEPone)Cl^- reduction shifted more negatively with chloride concentration, indicating that the reduction product $Mn(OEPone)^-$ was uncoordinated. The voltammetric results show that the manganese porphinones and porphinediones are reduced at significantly lower potentials than their manganese octaethylporphyrin analogue. The $E_{1/2,1}$ for the Mn(III)/Mn(II) reduction was decreased by 231 mV in going from the OEP to the OEPdione ligand. This was roughly the same amount as the Fe^{III} to Fe^{II} potentials (290 mV from OEP to OEPdione) [3]. The reduction potentials of the M^{II} porphyrin complexes were less dependent on the macrocycle when the metal was cobalt or iron. Like zinc porphyrins, the M^{II} reduction potential was significantly decreased for the porphinone and porphinediones complexes, as compared to Mn^{II}(OEP). As with zinc, the Mn^{II}(OEPdione) was reduced at a more negative potential than Mn^{II}(OEPone), though the shift was significantly larger than the DFT predicted value (experimental: 290 mV; DFT: 21 mV). This difference may be due to the differences in the formation constants for Cl^- with Mn^{II}(P). Coordination with Cl^- was not included in the DFT calculation. Limited solubility of the

chloride salt in THF prevented an accurate determination of the formation constants.

3.6. Visible spectroelectrochemistry of manganese porphinones

The electroreduction of manganese porphyrin and porphinone complexes occurred in two one-electron steps within the potential region that was studied. The visible data for the spectroelectrochemical reduction of Mn^{III}(OEPone)Cl are summarized in Table 2. Mn^{III}(OEPone)Cl gave a typical split Soret band (364 and 478 nm) for this metal. Split Soret bands were also observed for Mn^{III}(OEP)Cl. Upon reduction, a single Soret band was observed at 440 nm, and there was an increase in absorbance in the Q band at 624 nm. Because chloride was not added to the spectroelectrochemical solutions, Mn^{II}(P) was not coordinated with chloride. Further reduction led to a significant attenuation in the Soret band, and new band appeared at 444 nm (Fig. S5). In the Q band region, the band at 624 nm was bleached with a broad band appearing at 680 nm. A broad band from 600 to 800 nm was observed for $Mn(OEPone)^{-}$. This band was more pronounced in $Mn(OEPone)^{-}$ than in $Zn(OEPone)^{-}$, and is typical of a π-radical species.

The visible spectral changes during the first reduction of Mn^{III}(OEPdione)Cl are shown in Fig. 6A. The typical split Soret band of the manganese(III) complex gave rise to a strong Soret band at 464 nm, with two weaker bands at 402 and 436 nm. In the Q band region, the band shifted from 646 to 628 nm. As before, isosbestic points were observed. Further reduction of the manganese complex is shown in Fig. 6B. The Soret band at 464 nm disappeared, leaving a broad mostly featureless Soret band. The Q band at 628 nm also disappeared, and was replaced by a broad band at 680 nm, as seen with $Mn(OEPone)^{-}$.

Journal of Electroanalytical Chemistry, Vol. 744 (May 1, 2015): pg. 17-24. DOI.

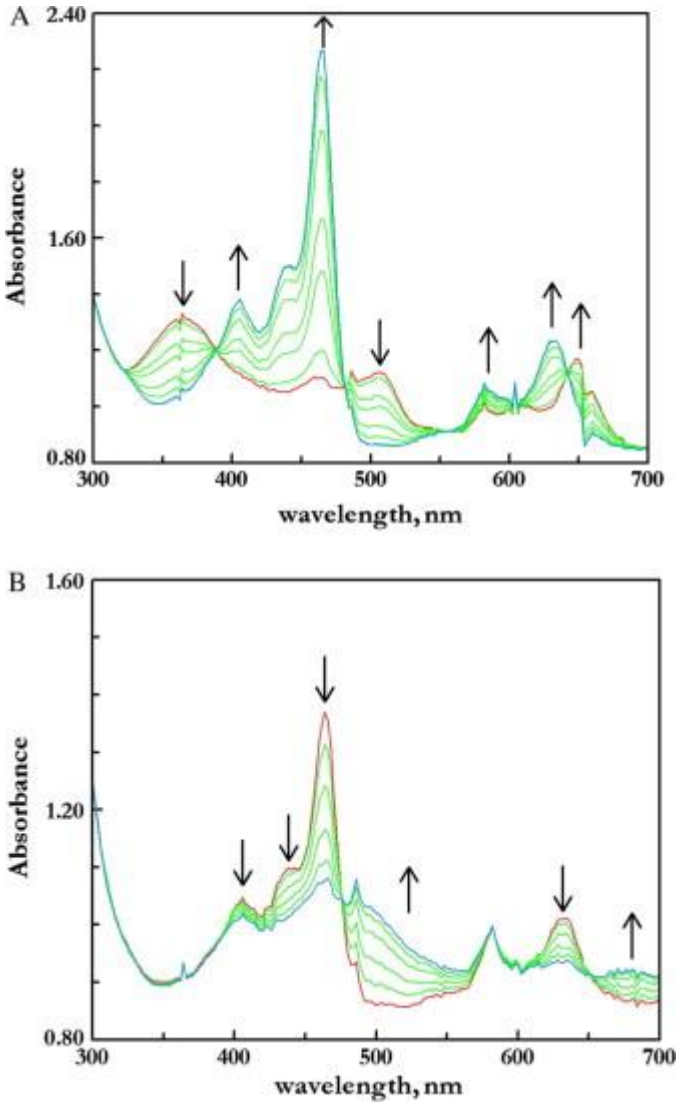

Fig. 6. Visible spectroelectrochemistry for the first (A) and second (B) reduction of 0.80 mM Mn(OEPdione)Cl in THF with 0.10 M TBAP. Red line is the initial scan; blue line is the final scan; green lines are the intermediate spectra. (A) Scan rate = 5.0 mV/s; E_i = 0.2 V; E_f = −0.6 V vs. Ag wire. (B) Scan rate = 5.0 mV/s; E_i = −0.6 V; E_f = −1.6 V vs. Ag wire. (For interpretation of the references to colour in this figure legend, the reader is referred to the web version of this article.)

3.7. Infrared spectroelectrochemistry manganese porphinones

The infrared spectrum of Mn^{III}(OEPone)Cl showed a carbonyl vibration at 1721 cm^{-1}. Additional bands were observed at 1578, 1570 and 1542 cm^{-1} (Fig. 7). Upon reduction at a potential between the first and second wave of manganese porphinone, the carbonyl band shifted

to 1707 cm^{-1}. Further reduction beyond the second wave gave rise to a downshift of the carbonyl band to 1657 cm^{-1} (Fig. 8). New bands were observed in the 1500 cm^{-1} region. The results are summarized in Table 3. As before, the starting spectra were regenerated upon oxidation.

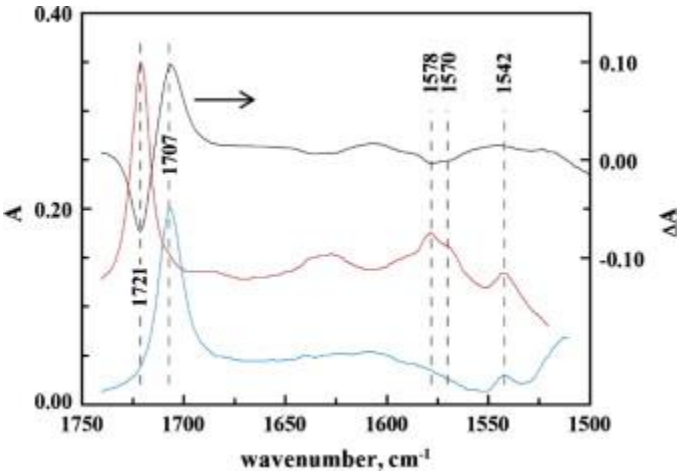

Fig. 7. Infrared spectroelectrochemistry for the first reduction of 3.0 mM Mn(OEPone)Cl in THF with 0.10 M TBAP. Red line: spectrum of Mn(OEPone)Cl (background subtracted); blue line: spectrum of Mn(OEPone); black line is the difference spectrum between the Mn(OEPone)Cl and Mn(OEPone); E = −0.60 V vs. Ag wire. (For interpretation of the references to colour in this figure legend, the reader is referred to the web version of this article.)

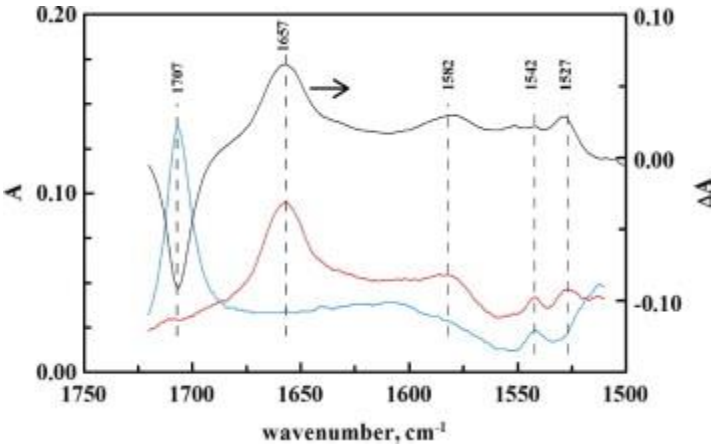

Fig. 8. Infrared spectroelectrochemistry for the second reduction of 3.0 mM Mn(OEPone)Cl in THF with 0.10 M TBAP. Blue line: spectrum of Mn(OEPone) (background subtracted); red line: spectrum of $Mn(OEPone)^{-}$; black line is the difference spectrum between the $Mn(OEPone)^{-}$ and Mn(OEPone); E = −1.60 V vs. Ag wire. (For interpretation of the references to colour in this figure legend, the reader is referred to the web version of this article.)

The infrared spectroelectrochemistry of Mn^{III}(OEPdione)Cl are shown in Fig. 9 and Fig. 10. The starting complex (Fig. 9) had two carbonyl bands at 1726 and 1718 cm^{-1}. On reduction, a broad carbonyl band was observed at 1707 cm^{-1}, which could be deconvoluted to two bands (1704 and 1710 cm^{-1}). The bands at 1595 and 1570 cm^{-1}, present in manganese(III) complex, disappeared. Further reduction (Fig. 10) caused additional downshift in the carbonyl band to 1693 cm^{-1}. New bands were observed at 1600, 1568 and 1552 cm^{-1}.

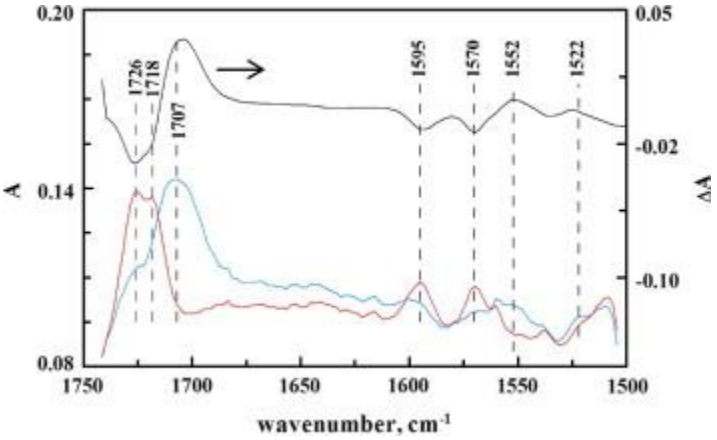

Fig. 9. Infrared spectroelectrochemistry for the first reduction of 3.0 mM Mn(OEPdione)Cl in THF with 0.10 M TBAP. Red line: spectrum of Mn(OEPdione)Cl (background subtracted); blue line: spectrum of Mn(OEPdione); black line is the difference spectrum between the Mn(OEPdione)Cl and Mn(OEPdione); E = −0.60 V vs. Ag wire. (For interpretation of the references to colour in this figure legend, the reader is referred to the web version of this article.)

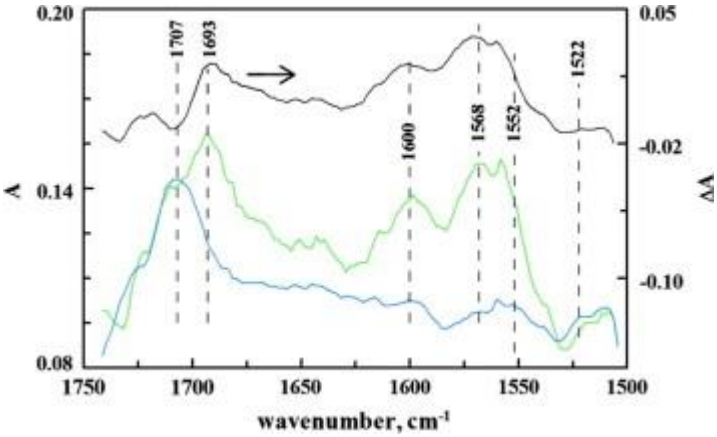

Fig. 10. Infrared spectroelectrochemistry for the second reduction of 3.0 mM Mn(OEPdione)Cl in THF with 0.10 M TBAP. Blue line: spectrum of Mn(OEPdione) (background subtracted); green line: spectrum of $Mn(OEPdione)^{-}$; black line is the difference spectrum between the $Mn(OEPdione)^{-}$ and Mn(OEPdione); E = −1.60 V vs.

Ag wire. (For interpretation of the references to colour in this figure legend, the reader is referred to the web version of this article.)

3.8. DFT calculations of the infrared spectra of manganese porphinones

The ν_{CO} bands for Mn(OEPone)Cl and Mn(OEPdione)Cl agreed well with the values predicted by DFT/m06 calculations (Table 4). Two bands were observed for Mn(OEPdione)Cl as predicted by the calculations. Upon reduction (Mn(III) to Mn(II)), the ν_{CO} bands of the octaethylporphinone complex decreased by 14 cm^{-1}, compared to the predicted value of 7 cm^{-1}. Similarly, the ν_{CO} band for Mn(OEPdione)Cl decreased by 16 and 14 cm^{-1} (DFT: 10 and 15 cm^{-1}). A decrease in the splitting of the carbonyl vibrations from 8 to 6 cm^{-1} was predicted by DFT calculations (15–10 cm^{-1}).

The reduction of Mn^{II}(OEPone) to Mn(OEPone)$^-$ caused a further decrease by 50 cm^{-1} (55 cm^{-1} by DFT). For the Mn^{II}(OEPdione), the downshifts were qualitatively similar to the shifts observed for Zn(OEPdione) reduction. Based on the DFT/m06 calculations, one carbonyl vibration downshifted 1710 to 1600 cm^{-1} (by 110 cm^{-1}), while the second one dropped from 1704 to 1693 cm^{-1} (by 11 cm^{-1}). This compares to the values predicted for a high-spin Mn^{II}(OEPdione)$^-$ of 23 and 124 cm^{-1}. The d-orbital occupancies of Mn(OEPdione)$^-$, as predicted by NBO theory, was essentially unchanged ($d^{5.19}$ vs. $d^{5.17}$). The spin density plot for Mn(OEPdione)$^-$ is shown in Fig. 4B. The spin-densities on the carbonyls are somewhat larger than the zinc complex, and with significantly less spin density on the left carbonyl. Calculations were also carried out for a low-spin complex. For Mn(OEPone)$^-$, the infrared spectrum was essentially the same as the high-spin complex, but the reduction was metal-based, leading to a Mn(I) complex ($d^{5.78}$). On the other hand, the low-spin spectrum of Mn(OEPdione)$^-$ was both qualitatively and quantitatively different from the high spin spectrum. Rather than a large splitting of the carbonyl bands, as was observed experimentally (193 cm^{-1}), both carbonyl bands downshifted significantly (1665 and 1651 cm^{-1}, splitting = 14 cm^{-1}). In addition, a Mn(I) complex was again formed ($3d^{5.81}$).

The m06 functional gave structures and spectra that agreed well with the experimental data. The bp86 functional predicted more of the reduction centered on the metal (more like a Mn^{I} structure; $d^{5.20}$ vs. $d^{5.43}$). It also predicted that one carbonyl should have decreased to 1635 cm^{-1}, with the second band at 1619 cm^{-1}, a much smaller splitting than observed. In addition, a very rich IR spectrum was predicted between 1500 and 1700 cm^{-1}.

For $Mn(OEPone)^{-}$, the ν_{CO} bands that were predicted for m06 functional (1654 cm^{-1}) were not significantly different from the bp86 functional (1648 cm^{-1}). As a result, it is not possible to assign the electron configuration of $Mn(OEPone)^{-}$ by the ν_{CO} alone. The other vibrations though are much more consistent with the m06 (π-radical anion) structure. The observed $Mn(OEPone)^{-}$ bands occurred at 1582, 1542 and 1527 cm^{-1} (Fig. 8). The spectrum predicted by the m06 functional (1552, 1542 and 1525 cm^{-1}) more closely matched the qualitative and quantitative spectrum than the bp86 predicted spectrum (1617, 1595, 1567 and 1555(s) cm^{-1}). The HOMO predicted for $Mn(OEPone)^{-}$ closely matched the shape of that predicted for $Mn(OEPdione)^{-}$. Thus, while the ν_{CO} bands are not as definitive for the electronic structure, the overall spectrum corresponds well to a π-radical anion complex.

3.9. Comparison with Fe/Co porphinones

The results for zinc and manganese porphinones indicate that the dione complexes provide the most significant information on the electronic state of the anion. The formation of π-radical anion porphinediones leads to the filling of the π^{*}-orbital which has greater density on one carbonyl as opposed to the other. Previous studies have been reported on iron and cobalt porphinones, along with DFT calculations [14] and [15]. These calculations were carried out using the bp86 functional. We have repeated these calculations using the m06 functional, and the results are shown in Table 4. Unlike the zinc and manganese porphinedione anions, the experimental ν_{CO} bands had a relatively small splitting in the $M(OEPdione)^{-}$ complex (5 cm^{-1} for Fe, 15 cm^{-1} for Co). These results are qualitatively different from the Zn and Mn porphinedione results. The DFT calculation for $Fe(OEPdione)^{-}$ with the m06 functional predicted the a π-radical anion Fe(II) complex.

Journal of Electroanalytical Chemistry, Vol. 744 (May 1, 2015): pg. 17-24. DOI.

In addition, it predicted a large splitting in the ν_{CO} bands of $Fe(OEPdione)^-$ (43 cm^{-1}) with one ν_{CO} band downshifting little upon reduction (8 cm^{-1}). This prediction was very similar to the behavior of the zinc and manganese complexes. The predicted ν_{CO} splitting was less than that observed for $Mn/Zn(OEPdione)^-$, but significantly greater than the experimental values. On the other hand, the bp86 functional predicted a small splitting of the ν_{CO} vibrations (12 cm^{-1}), and a significant decrease in both ν_{CO} vibrations upon reduction (34 and 46 cm^{-1}). As was observed with $Mn(OEPdione)^-$, the bp86 functional favored a metal reduction ($Fe^{I}(OEPdione)^-$, $d^{6.82}$), and was in this case more consistent with the experimental data. The spin density plot for $Fe^{I}(OEPdione)^-$ is shown in Fig. 4C. While the m06 functional predicted a π-radical anion, the lower splitting of the ν_{CO} bands as compared to the Zn/Mn complexes (43 vs. 78/91 cm^{-1}), and the NBO occupancy ($3d^{6.62}$) indicates that there was considerable Fe(I) character in the complex. By contrast, the m06 functional predicted a $Co^{I}(OEPdione)^-$ structure. As was observed in $Fe(OEPdione)^-$, both ν_{CO} bands decreased but the m06 functional predicted a larger decrease (62 and 71 cm^{-1}) than observed (26 and 41 cm^{-1}).

4. Conclusions

This work has shown that infrared spectroelectrochemistry in combination with DFT calculations can allow us to deduce the electronic structure of the reduction product. This was clearly the case with metalloporphinediones, where the behavior of the two carbonyl groups upon reduction of the complex can allow the characterization of the complex. In particular, for π-radical anion complexes, reduction of the complex led to a large splitting of the ν_{CO} bands because one carbonyl was affected much more than the second because of the shape of the π^* orbital. For metal reductions, both carbonyl groups decreased in energy by similar amounts, due to backbonding by the central metal. This leads to a qualitative and quantitative difference in the infrared spectrum.

In addition, it was found that the m06 functional favored ligand centered reduction, while the bp86 functional favored metal centered reduction. It was only by comparison with the experimental data for the metalloporphinediones that it was possible to decide which

Journal of Electroanalytical Chemistry, Vol. 744 (May 1, 2015): pg. 17-24. DOI.

functional was most accurate. On the other hand, for the metalloporphinones, such a distinction was not possible, as both functionals predicted similar spectra, even though the electronic structures were different.

Appendix A. Supplementary material

Table of Contents.

Figure S1. Predicted carbonyl frequencies for M(III) and M(II) porphinones using m06 functional as compared for experimental wavenumbers. Experimental data from this work and Ref. [1, 2]. Trendline has a slope of 1.06.

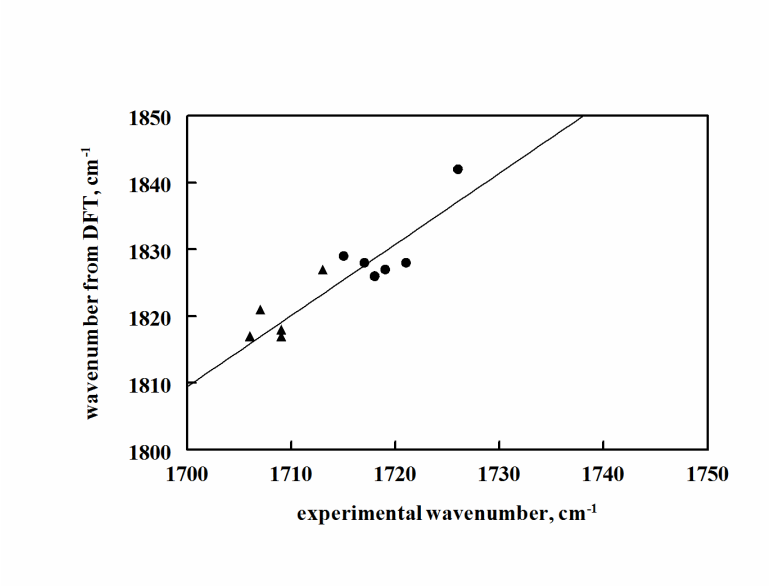

Figure S2. Visible spectroelectrochemistry for the reduction of 0.80 mM Zn(OEPone) in THF with 0.10 M TBAP. Solid red line is the initial scan; solid blue line is the final scan; solid green lines are the intermediate spectra. Scan rate = 8.2 mV/s; E_i = -0.30 V; E_f = -1.81 V vs. Ag wire.

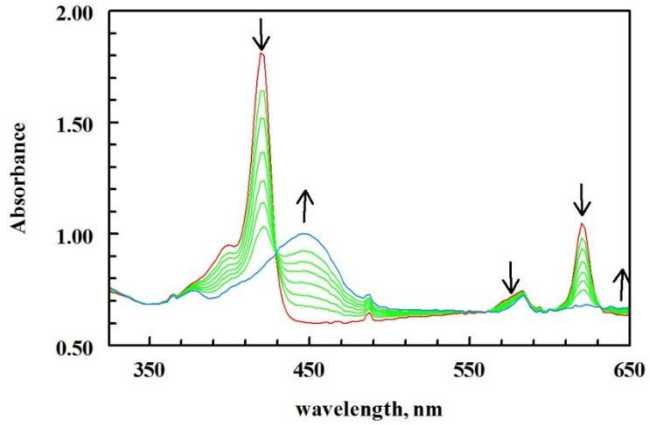

Figure S3. Infrared spectrum for $Zn(OEPone)^-$ using Gaussian G09 with DFT and m06 (red) and bp86 (blue) functionals.

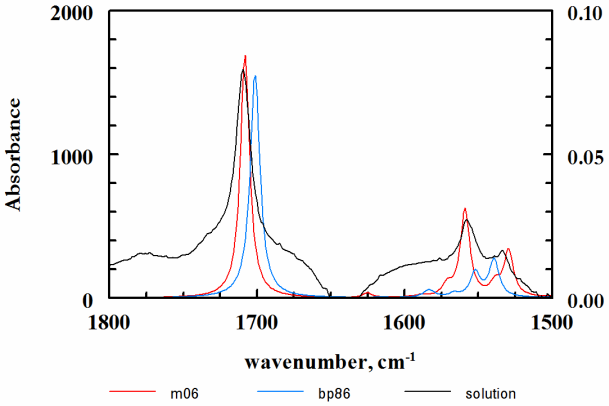

Figure S4. Spin density plot for $Zn(OEPone)^-$ from the DFT calculations using the m06 functional.

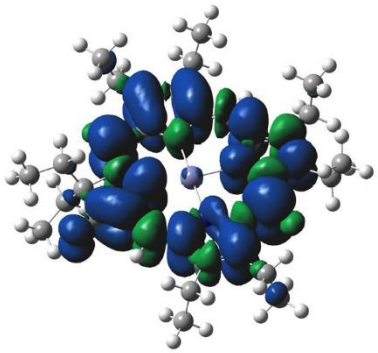

Figure S5. Visible spectroelectrochemistry for the second reduction of 0.80 mM Mn(OEPone)Cl in THF with 0.10 M TBAP. Solid red line is the initial scan; solid blue line is the final scan; solid green lines are the intermediate spectra. Scan rate = 8.0 mV/s; E_i = -0.6 V; E_f = -1.5 V vs. Ag wire.

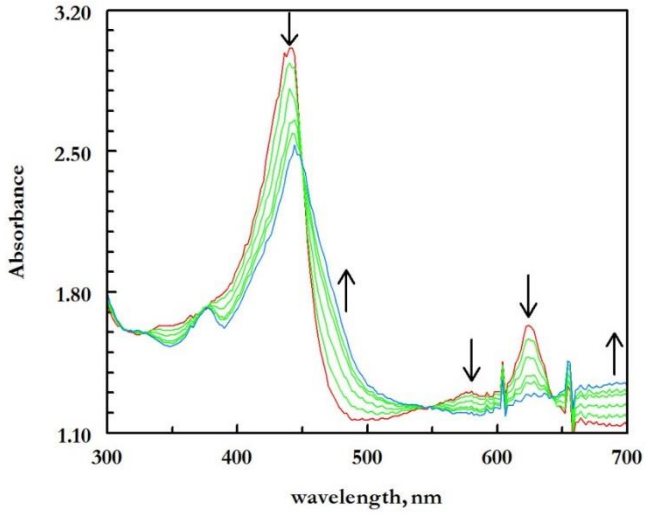

Figure S6. Molecular orbital for $Mn(OEPdione)^{-}$ (A_{1u}).

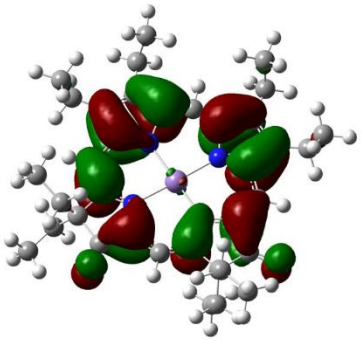

Reference List

1. F. Tutunea, M. D. Ryan, J. Electroanal. Chem., 670 (2012) 16.
2. Z. Wei, M. D. Ryan, Inorg. Chem., 49 (2010) 6948.

References

[1] C.K. Chang. J. Biol. Chem., 260 (1985), pp. 9520–9522
[2] Y.M. Liu, C. DeSilva, M.D. Ryan. Inorg. Chim. Acta, 258 (1997), pp. 247–255
[3] Y. Liu, M.D. Ryan. Inorg. Chim. Acta, 225 (1994), pp. 57–66
[4] P. Doppelt, J. Fischer, R. Weiss. Inorg. Chem., 23 (1984), pp. 2958–2962
[5] J.G. Lanese, G.S. Wilson. J. Electrochem. Soc., 119 (1972), pp. 1039–1043
[6] G. Balducci, G. Chottard, C. Gueutin, D. Lexa, J.M. Saveant. Inorg. Chem., 33 (1994), pp. 1972–1978
[7] S. Hu, C.-Y. Lin, M.E. Blackwood Jr., A. Mukherjee, T.G. Spiro. J. Phys. Chem., 99 (1995), pp. 9694–9701
[8] R.A. Reed, R. Purrello, K. Prendergast, T.G. Spiro. J. Phys. Chem., 95 (1991), pp. 9720–9727
[9] J.H. Fuhrhop, K.M. Kadish, D.G. Davis. J. Am. Chem. Soc., 95 (1973), pp. 5140–5147
[10] S.L. Kelly, K.M. Kadish. Inorg. Chem., 21 (1982), pp. 3631–3639

[11] L.J. Boucher, H.K. Garber. Inorg. Chem., 9 (1970), pp. 2644–2649
[12] D.M. Guldi, M. Kumar, P. Neta, P. Hambright. J. Phys. Chem., 96 (1992), pp. 9576–9581
[13] M.S. Liao, J.D. Watts, M.J. Huang. Inorg. Chem., 44 (2005), pp. 1941–1949
[14] F. Tutunea, M.D. Ryan. J. Electroanal. Chem., 670 (2012), pp. 16–22
[15] Z. Wei, M.D. Ryan. Inorg. Chem., 49 (2010), pp. 6948–6954
[16] C.K. Chang, C. Sotiriou. J. Org. Chem., 50 (1985), pp. 4989–4991
[17] C.K. Chang, C. Sotiriou, W. Wu. J. Chem. Soc., Chem. Commun. (1986), pp. 1213–1215
[18] W. Wu, C.K. Chang. J. Am. Chem. Soc., 109 (1987), pp. 3149–3150
[19] C.K. Chang, C. Sotiriou. J. Org. Chem., 52 (1987), pp. 926–929
[20] X.Q. Lin, K.M. Kadish. Anal. Chem., 57 (1985), pp. 1498–1501
[21] M.J. Frisch, G.W. Trucks, H.B. Schlegel, G.E. Scuseria, M.A. Robb, J.R. Cheeseman, G. Scalmani, B. Barone, B. Mennucci, G.A. Petersson, H. Natatsuji, M. Caricota, X. Li, H.P. Hratchian, A.F. Izmaylov, J. Bloino, G. Zheng, J.L. Sonnenberg, M. Hada, K. Toyota, R. Fukuda, J. Hasegawa, M. Ishida, T. Nakajima, Y. Honda, O. Kitao, H. Nakai, T. Vreven, J.A. Montgomery Jr., J.E. Peralta, F. Ogliaro, M. Bearpark, J.J. Heyd, E. Brothers, K.N. Kudin, V.N. Staroverov, R. Kobayashi, J. Normand, K. Raghavachari, A. Rendell, J.C. Burant, S.S. Iyengar, J. Tomasi, M. Cossi, N. Rega, N.J. Millam, M. Klene, J.E. Knox, J.B. Cross, V. Bakken, C. Adamo, J. Jaramillo, R. Gomperts, R.E. Stratmann, O. Yazyev, A.J. Austin, R. Cammi, C. Pomelli, J.W. Ochterski, R.L. Martin, K. Morokuma, V.G. Zakrzewski, G.A. Voth, P. Salvador, J.J. Dannenberg, S. Dapprich, A.D. Daniels, Ö. Farkas, J.B. Foresman, J.V. Ortiz, J. Cioslowski, D.J. Fox. Gaussian Inc. Wallingford, CT (2009)
[22] A.J.H. Wachters. J. Chem. Phys., 52 (1970), pp. 1033–1036
[23] J.P. Holland, J.C. Green, J.R. Dilworth. Dalton Trans. (2006), pp. 783–794
[24] A.M. Stolzenberg, P.A. Glazer, B.M. Foxman. Inorg. Chem., 25 (1986), pp. 983–991
[25] K.M. Kadish, S. Kelly. Inorg. Chem., 18 (1979), pp. 2968–2971
[26] X.H. Mu, F.A. Schultz. Inorg. Chem., 34 (1995), pp. 3835–3837